frontiers | Frontiers in Physiology

TYPE Original Research
PUBLISHED 25 April 2025
DOI 10.3389/fphys.2025.1555230

OPEN ACCESS

EDITED BY
Aranyak Chakravarty,
Jadavpur University, India

REVIEWED BY
Mehrdad Behnia,
University of Central Florida, United States
Hans Haverkamp,
Washington State University Health Sciences Spokane, United States

*CORRESPONDENCE
Ching-Long Lin,
ching-long-lin@uiowa.edu

RECEIVED 03 January 2025
ACCEPTED 14 April 2025
PUBLISHED 25 April 2025

CITATION
Li F, Zhang X, Comellas AP, Hoffman EA, Graham MM and Lin C-L (2025) Longitudinal study of COPD phenotypes using integrated SPECT and qCT imaging.
Front. Physiol. 16:1555230.
doi: 10.3389/fphys.2025.1555230

Longitudinal study of COPD phenotypes using integrated SPECT and qCT imaging

Frank Li[1,2], Xuan Zhang[2,3], Alejandro P. Comellas[4], Eric A. Hoffman[1,5], Michael M. Graham[5] and Ching-Long Lin[1,2,3,5]*

[1]Roy J. Carver Department of Biomedical Engineering, University of Iowa, Iowa City, IA, United States, [2]IIHR-Hydroscience and Engineering, University of Iowa, Iowa City, IA, United States, [3]Department of Mechanical Engineering, University of Iowa, Iowa City, IA, United States, [4]Department of Internal Medicine, University of Iowa, Iowa City, IA, United States, [5]Department of Radiology, University of Iowa, Iowa City, IA, United States

Introduction: The aim of this research is to elucidate chronic obstructive pulmonary disease (COPD) progression by quantifying lung ventilation heterogeneities using single-photon emission computed tomography (SPECT) images and establishing correlations with quantitative computed tomography (qCT) imaging-based metrics. This approach seeks to enhance our understanding of how structural and functional changes influence ventilation heterogeneity in COPD.

Methods: Eight COPD subjects completed a longitudinal study with three visits, spaced about a year apart. CT scans were performed at each visit and qCT-based variables were derived to measure the structural and functional characteristics of the lungs, while the SPECT-based variables were used to quantify lung ventilation heterogeneity. The correlations between key qCT-based variables and SPECT-based variables were examined.

Results: The SPECT-based ventilation heterogeneity (CV_{Total}) showed strong correlations with the qCT-based functional small airway disease percentage ($fSAD\%_{Total}$) and emphysematous tissue percentage ($Emph\%_{Total}$) in the total lung, based on cross-sectional data. Over the 2-year period, changes in SPECT-based hot spots (TC_{Max}) exhibited strong negative correlations with changes in $fSAD\%_{Total}$, $Emph\%_{Total}$, and the average airway diameter in the left upper lobe, as well as a strong positive correlation with alternations in airflow distribution between the upper and lower lobes.

Discussion: In conclusion, this study found strong positive cross-sectional correlations between CV_{Total} and both fSAD% and Emph%, suggesting that these markers primarily reflect static disease severity at a single time point. In contrast, longitudinal correlations between changes in TC_{Max} and other variables over 2 years may capture the dynamic process of hot spot formation, independent of disease severity. These findings suggest that changes in TC_{Max} may serve as a more sensitive biomarker than changes in CV_{Total} for tracking the underlying mechanisms of COPD progression.

KEYWORDS

CT, SPECT, COPD, ventilation, small airway disease

Introduction

Chronic obstructive pulmonary disease (COPD) is a prevalent respiratory disease that imposes a significant burden on healthcare systems worldwide (Halpin et al., 2022). The Global Initiative for Chronic Obstructive Lung Disease (GOLD) report (Global Strategy For Prevention, 2023) has been continuously updated to better characterize the heterogeneities of COPD and improve treatment outcomes (Ferrera et al., 2021; Vogelmeier et al., 2020). In addition, imaging modalities, such as computed tomography (CT) and single-photon emission computed tomography (SPECT), have been utilized to visualize and quantify regional functional and structural changes associated with various pathological processes in lung diseases, such as emphysema (Israel et al., 2019).

Innovative biomarkers based on quantitative CT (qCT) imaging have been developed to investigate the underlying causes of COPD. These biomarkers assess a wide range of risk factors and associated defects, such as airway-branch variation (Smith et al., 2018), dysanapsis (Smith et al., 2020), and pulmonary vascular dysfunction (Alford et al., 2010; Iyer et al., 2016). The introduction of the qCT-based parametric response map has significantly advanced research on functional small airway disease (fSAD) and emphysema (Emph) (Galbán et al., 2012). Both fSAD and Emph are critical phenotypes in COPD, with the former considered a precursor to the latter (Ostridge et al., 2016). It is suggested that targeting small airways with appropriate treatments may potentially control the progression of both airway and parenchymal diseases in COPD (Singh, 2017). Novel multiscale qCT biomarkers have been developed to capture a wide range of phenotypes at various stages of lung disease (Choi et al., 2015). These imaging-based biomarkers enable the identification of unique structural and functional features within COPD subgroups, exhibiting strong associations with distinct clinical characteristics. For instance, Haghighi et al. applied unsupervised clustering techniques to cross-sectional qCT biomarkers and identified four clinically relevant subgroups among former and current smokers, respectively (Haghighi et al., 2018a; Haghighi et al., 2019a). In addition, Zou et al. analyzed longitudinal qCT biomarkers to study COPD progression (Zou et al., 2021a).

SPECT ventilation imaging allows for the assessment of global and regional lung ventilation by measuring the concentration of a radioactive tracer. This tracer acts as a biomarker for ventilation, provided that the aerosol size of the tracer is small enough to reach the alveoli. De Backer et al. demonstrated a strong correlation between CT-based lobar air volume change and lobar SPECT tracer aerosol concentration with aerosol diameter less than 2 μm (De Backer et al., 2010). They further demonstrated that the hot spots observed on SPECT images corresponded to airway narrowing on CT images. Studies have also demonstrated a correlation between heterogeneities observed on SPECT images and impaired lung functions. Xu et al. found that the coefficient of variation (CV) observed in SPECT images, a measure of ventilation heterogeneity, not only differentiated patients with emphysema from non-emphysematous smokers and non-smokers, but also correlated with pulmonary functions (Xu et al., 2001). Thus, combining SPECT and CT imaging allows for a comprehensive evaluation of both functional and structural relationships within different regions of the lungs (Israel et al., 2019).

In this study, we aimed to evaluate COPD progression by quantifying structural and functional changes in CT and SPECT images of COPD subjects acquired at three visits, approximately 1 year apart. Our objective was to establish connections between qCT-based variables and SPECT-based biomarkers to better understand how structural and functional alterations interact both cross-sectionally and longitudinally during COPD progression, offering new insights into ventilation heterogeneities. We hypothesized that qCT-based structural and functional alterations correlate with SPECT-measured functional ventilation characteristics in COPD. While this correlation was anticipated, it had never been established or quantified *in vivo*.

Materials and methods

Fourteen subjects were initially recruited for a longitudinal study with three visits at baseline (V0), 12.84 ± 1.68 months (V1), and 26.20 ± 3.06 months (V2). The inclusion criteria were as follows: current or former smokers with at least a 10 pack-year smoking history, who have been classified as a COPD GOLD 0-4. Five subjects dropped out due to other health issues or personal reasons, and one subject was excluded due to an abnormal airway structure with an accessary bronchus connected to the right main bronchus. Thus, eight subjects who completed all three visits were analyzed in this study. Pulmonary function tests (PFTs, see Supplementary Material/Content 1; Supplementary Figure S1 for more details), CT scans, and SPECT scans were acquired at each visit. This study was approved by the institutional review board of the University of Iowa and the informed consent was obtained from all the patients before the study.

CT images and qCT variables

Three static three-dimensional (3D) CT scans were acquired using the Siemens SOMATOM Force Scanner at the lung volumes of total lung capacity (TLC), functional residual capacity (FRC) and residual volume (RV). The lung volume control system used was the same as that employed in the previous study (Fuld et al., 2012). The TLC scan protocol used dose modulation with 36 reference mAs, 120 kV, pitch of 1.0, and rotation time of 0.25 s. The FRC and RV scans used dose modulation with 15 reference mAs, 120 kV, pitch of 1.0, and rotation time of 0.25 s. The CT images have a spatial resolution of 0.5 mm in the z-axis, and 0.5–0.7 mm in the x and y-axes. The subjects were positioned on the CT table in the supine position and were instructed to breathe normally through the mouthpiece for a few breathing cycles. While the CT scans were performed, they were instructed to take in a deepest breath and hold it at the desired lung volume of TLC, FRC, or RV. The subject breathed normally for several cycles before the next CT scan was performed. Repeatability tests assessing qCT measures have demonstrated excellent reliability and reproducibility (Motahari et al., 2023).

The CT images were processed using VIDA Vision (VIDA Diagnostics Inc., Coralville, Iowa) to segment the lung, lobes, and airways. A mass preserving image registration technique

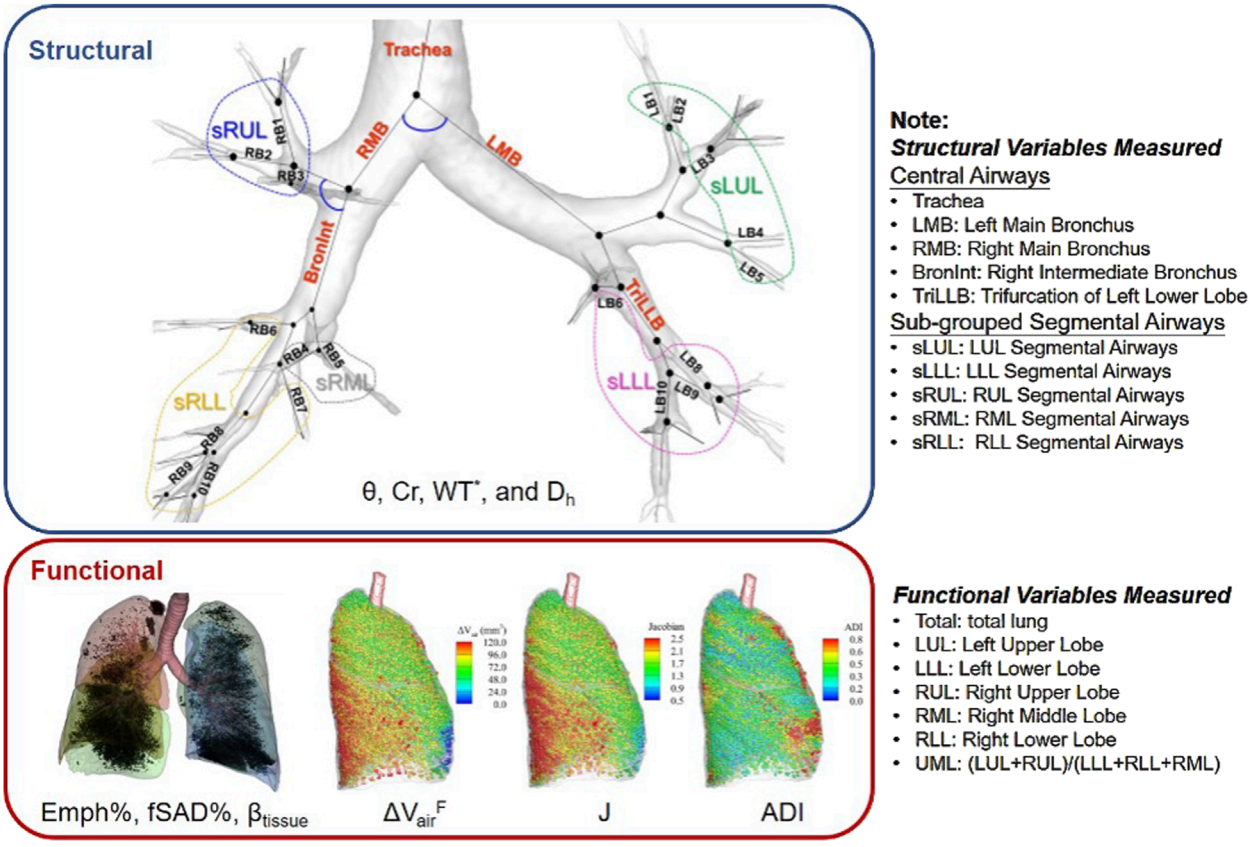

FIGURE 1
The multiscale structural and functional qCT variables.

was performed to match FRC (or RV) with TLC images (Haghighi et al., 2018b). TLC and RV images were registered to derive functional variables, while TLC and FRC images were registered to match SPECT images. A total of 69 structural and functional multiscale qCT variables presented in previous studies were derived (Haghighi et al., 2018a; Haghighi et al., 2019a; Zou et al., 2021a) as shown in Figure 1. Please refer to Supplementary Material/Content 2 for a detailed explanation of these variables, and to Content 3 for a list of abbreviations of qCT variables. The structural variables describe regional alterations in lung structures, while the functional variables capture changes in regional lung function. The qCT variables most relevant to this study include normalized airway wall thickness (WT^*), normalized airway hydraulic diameter (D_h^*), fractional air volume change (ΔV_{air}^F), determinant of Jacobian matrix (J), anisotropic deformation index (ADI), fraction-based small airways disease (fSAD%), fraction-based emphysema (Emph%), and tissue fraction at TLC (β_{tissue}). Specifically, the wall thickness and hydraulic diameter were normalized, as indicated by an asterisk, using predicted values from healthy subjects to account for inter-subject variability related to sex, age, and height (Choi et al., 2015). ΔV_{air}^F represents the ratio of the air-volume change in the lobes to the total air-volume change in the whole lung, while $\Delta V_{air,UML}^F$ represents the ratio of the air-volume change in the upper lobes to the air-volume change in the combined middle and lower lobes.

The region where the qCT variable was measured is indicated as a subscript of the variable, formatted as $\{Variable\}_{\{Region\}}$. The structural variables were measured from the lung shape, central airways, and segmental airways. The lung shape was measured at TLC as the ratio of apical-basal distance and ventral-dorsal distance. The central airways include trachea, left main bronchus (LMB), right main bronchus (RMB), right intermediate bronchus (BronInt), and trifurcation of left lower lobe (TriLLB). The segmental airways were grouped by lobes, such as sub-grouped segmental airways of left upper lobe (sLUL), sub-grouped segmental airways of left lower lobe (sLLL), sub-grouped segmental airways of right upper lobe (sRUL), sub-grouped segmental airways of right middle lobe (sRML), and sub-grouped segmental airways of right lower lobe (sRLL). The functional variables were measured at lobar level, including left upper lobe (LUL), left lower lobe (LLL), right upper lobe (RUL), right middle lobe (RML), and right lower lobe (RLL), as well as total lung level (Total).

SPECT images and variables

The subject was positioned supine on the SPECT scanner to replicate the positioning used in the above CT scans. The subject inhaled ^{99m}Tc sulfur colloid, a radioactive tracer aerosol generated by a specialized nebulizer, through a mouthpiece with

the nose occluded. A 3D SPECT scan of the whole lung was then performed. The particle size of the sulfur colloid is below 1 μm (Krogsgaard, 1976), allowing the tracer aerosol to penetrate deep into the lung (Sirr et al., 1985). Since ^{99m}Tc sulfur colloid is non-absorbable, it is not rapidly cleared from the lungs. The 3D SPECT scan took approximately 20 min to complete and was acquired during continuous tidal breathing. The SPECT images have a spatial resolution of 3.895 mm along the x, y, and z-axes. The estimated radiation dose retained by the subject was 0.17 mSv, well below the U.S. Nuclear Regulatory Commission standard of 50 mSv/year. Initially, the SPECT imaging protocol involved using ^{99m}Tc-HMPAO labeled neutrophils to assess inflammation distribution. This method was used for the first two subjects at V0 but yielded minimal signal capture, as the ^{99m}Tc-HMPAO-labeled neutrophils moved too quickly through the pulmonary vessels. Consequently, we modified the protocol, which is why the first two subjects did not have SPECT ventilation scans at V0.

SPECT imaging is a dynamic process that produces time-averaged images during tidal breathing, while CT images are static scans acquired at TLC, FRC, and RV. It is preferable to match the SPECT images with the FRC CT images, as FRC represents a lung volume closer to tidal breathing, compared to RV or TLC. The lung deformation from FRC to the peak of tidal volume was assumed to be relatively small and quasi-linear. Thus, the SPECT images were first aligned with the FRC CT images using affine transforms, with mutual information as the cost function. Displacement fields for transforming the FRC CT images to TLC were then obtained through image registration. These displacement fields were subsequently applied to the SPECT images, deforming them to match the TLC CT images, which provide detailed anatomical information of the lungs.

After aligning the SPECT images with the TLC CT images, tracer concentrations (TC) within the lung and each lobe were quantified based on the domain of TLC CT images. The ratio of TC in a lobe over the total lung (TC%), the TC coefficient of variation for the total lung (CV_{Total}), and the standardized maximum TC in the total lung (TC_{Max}) were used to quantify the distribution, heterogeneity, and hot spots of TC. Specifically, TC% measured lobar ventilation distribution, while CV_{Total}, the ratio of the standard deviation to the average of TC (Xu et al., 2001), measured ventilation heterogeneity. TC_{Max} quantified the magnitude of local hot spots as an indicator of airway narrowing. The normalized CV_{Total} and TC_{Max} accounted for variations in the amount of TC inhaled. Moreover, the correlation between TC% and ΔV^F_{air} was used to assess the efficacy of the image registration of SPECT and CT images. Pearson's correlation coefficients (r) between CV_{Total} and PFT values were calculated and validated against previous studies (Xu et al., 2001; Nagao and Murase, 2002). Correlation strengths were categorized as follows: $|r| \leq 0.3$ as negligible, $0.3 < |r| \leq 0.5$ as weak, $0.5 < |r| \leq 0.7$ as moderate, $0.7 < |r| \leq 0.9$ as strong, and $|r| > 0.9$ as very strong.

Analysis of SPECT and qCT variables

The associations between SPECT and qCT variables were evaluated to enhance the interpretation of the SPECT variables. Exploratory factor analysis (EFA) was applied to reduce the extensive number of qCT variables derived from the 799 current and former smokers analyzed previously (Haghighi et al., 2018a; Haghighi et al., 2019a) to a smaller set of factors that preserved the variability of qCT-captured features. EFA identifies patterns or structures in a large set of variables by reducing them to a smaller number of factors, making complex data easier to interpret. The number of factors was determined using the parallel analysis (Horn, 1965). Factors were extracted using principal component analysis with Varimax orthogonal rotation (Kaiser, 1958) to ensure their independence.

We then identified key qCT variables that significantly contributed to each factor, using them as surrogates to interpret disease phenotypes. qCT variables were regarded as key if their loading values on their corresponding factors exceeded 0.6. We then examined the correlations between key qCT variables and SPECT variables, using cross-sectional data from V0, V1, and V2 as well as the longitudinal data showing changes between any two visits of V1 and V0 (V1-V0, 1 year apart), V2 and V1 (V2-V1, 1 year apart), and V2 and V0 (V2-V0, 2 years apart).

With small sample sizes, we prioritized large effect sizes (Pearson's coefficients >0.7) in this exploratory study (Akoglu, 2018; Cohen, 1992). This approach acknowledges two challenges of small samples: insufficient statistical power to detect real effects (increasing Type II errors) and vulnerability to spurious significance from random fluctuations. Importantly, statistical power can be deemed adequate with a smaller sample when the effect size is large (Shreffler and Huecker, 2023). By focusing on effect size, we quantified relationship magnitudes independent of sample size, ensuring the observed effects were substantial and meaningful despite limited data.

Result

The clinical data and PFT results for the eight COPD subjects are presented in Table 1 (see Supplementary Table S1 for more data). These subjects (age: 63.1 ± 11.5 years; range: 51–84 years) had an average Tiffeneau ratio [FEV_1/FVC (%)] of 52.9% ± 16.6% and an average predicted forced expiratory volume ratio (FEV_1% predicted) of 67.9% ± 16.3% at V0. The mean changes between V1 and V0 were 0.0% ± 1.9% for FEV_1/FVC (%) and −2.5% ± 5.4% for FEV_1 (%) predicted. Additionally, the mean changes between V2 and V1 were 0.8% ± 1.9% for FEV_1/FVC (%) and 3.5% ± 4.6% for FEV_1% predicted. Thus, the lung function of all subjects remained approximately stable over the 2-year period (Pellegrino et al., 2005).

At V0, Subjects 2 and 5 had moderate-to-severe (GOLD 2, bordering on GOLD 3) and severe (GOLD 3) airflow obstruction, respectively, according to their PFT results. Subjects 1, 3, and 4 had moderate (GOLD 2) airflow obstruction. Subject 6 had mild airflow obstruction (GOLD 1), while Subjects 7 and 8 were at risk of COPD (GOLD 0). Additionally, Subjects 1 through 5 were former smokers, while Subjects 6 through 8 were current smokers.

SPECT features

TC% and ΔV^F_{air} of each lobe at each visit are listed in Supplementary Table S2. The correlation coefficient between TC% and ΔV^F_{air} was 0.73, indicating a strong positive relationship between the two variables (Figure 2a). In addition, the correlations between

TABLE 1 Clinical data, PFT at V0, and changes in PFT between visits. Subjects 1–5 were former smokers, while Subjects 6–8 were current smokers.

Subject	Sex	Age (yrs.) at V0	BMI	GOLD stage	V0		V1 - V0		V2 - V0	
					FEV1% predicted	FEV1/FVC (%)	ΔFEV1% predicted	ΔFEV1/FVC (%)	ΔFEV1% predicted	ΔFEV1/FVC (%)
1	M	80	32	2	73	53	1	3	3	0
2	M	84	23	2	50	28	−11	−2	1	1
3	M	55	26	2	63	51	−2	0	−1	0
4	M	59	21	2	73	56	−5	2	5	4
5	M	59	32	3	36	28	−5	−3	−3	0
6	M	51	29	1	83	59	−5	−1	−2	0
7	F	54	27	0	77	71	−2	0	−4	0
8	F	63	36	0	88	77	9	1	9	1
Mean ± SD		63.1 ± 11.5	28.3 ± 4.7		67.9 ± 16.3	52.9 ± 16.6	−2.5 ± 5.4	0.0 ± 1.9	1.0 ± 4.2	0.8 ± 1.3

10.3389/fphys.2025.1555230

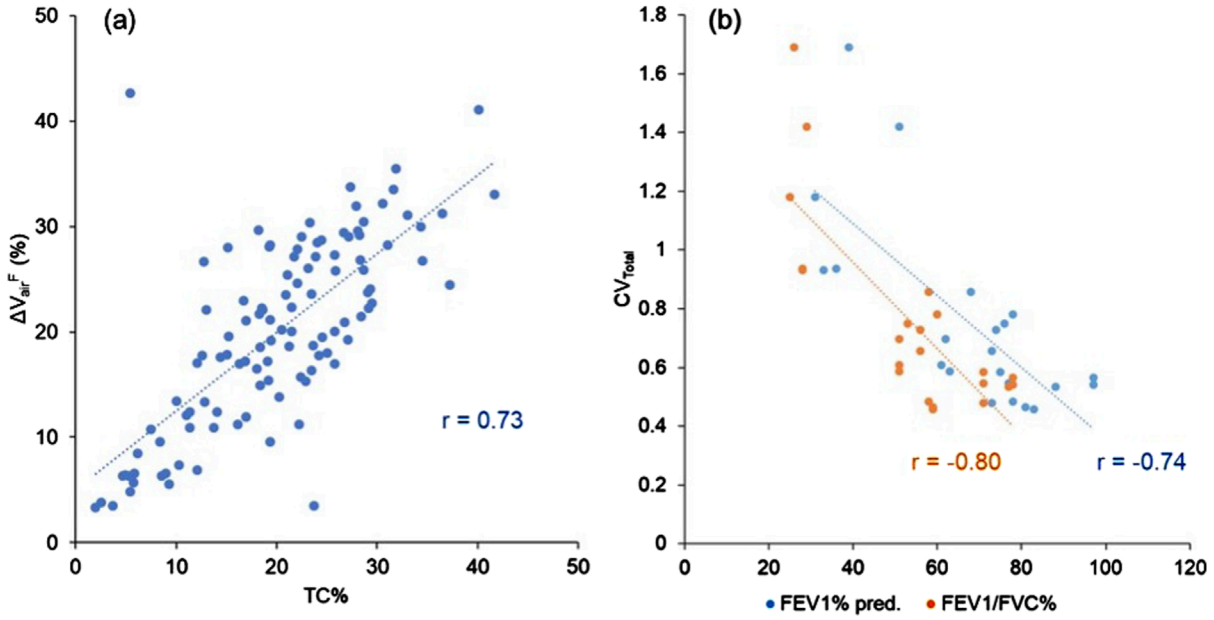

FIGURE 2
(a) A scatter plot showing the strong correlation between TC% and ΔV_{air}^{F} of the lobes (r = 0.73). **(b)** A scatter plot showing the strong correlations between CV_{Total} and PFT results (FEV_1% predicted: r = −0.74, FEV_1/FVC (%): r = −0.80). Data points are derived from all three visits.

CV_{Total} and PFT values revealed a strong negative correlation with FEV_1% predicted (r = −0.74) and an even stronger negative correlation with FEV_1/FVC (%) (r = −0.80) (Figure 2b).

The SPECT images for all the subjects are displayed in Figure 3. CV_{Total} and TC_{Max} at each visit, together with their changes between visits, are summarized in Table 2. Across all visits, these subjects were categorized into three distinct subgroups: (Global Strategy for Prevention, 2023; Israel et al., 2019), (Smith et al., 2018; Smith et al., 2020; Alford et al., 2010) and (Halpin et al., 2022; Ferrera et al., 2021; Vogelmeier et al., 2020). Subjects 2 and 5 were characterized by higher CV_{Total} and extremely elevated TC_{Max}. In contrast, Subjects 6, 7, and 8 exhibited more homogeneous TC distributions, while Subjects 1, 3, and 4 showed ventilation distribution patterns that fell between the other two subgroups. Notable hot spots, revealed by concentrated red areas, were evident in the SPECT images of Subjects 2 and 5 throughout all visits. A prominent hot spot was also observed on the left upper lobe in the SPECT image of Subject 3 at V2. The changes of CV_{Total} and TC_{Max} between visits were minimal for all subjects, around 10%.

Key qCT-based factors and variables

Seven factors, extracted from the qCT variables of former and current smokers (Choi et al., 2015; Haghighi et al., 2018a), accounted for 78.4% of the variance in the original features. Among all the qCT variables, ADI_{Total}, J_{Total}, $\beta_{tissue,Total}$, $fSAD\%_{Total}$, $D_h^*{}_{sLUL}$, $Emph\%_{Total}$, $\Delta V^F_{air,UML}$, WT^*_{sLLL}, and $D_h^*{}_{LMB}$ were the key qCT variables that contributed significantly to the factors and were selected for analysis in this study. The key qCT variables with moderate-to-high (factor loading = 0.6–0.7) and high contributions to the factors (factor loading >0.7) are listed in Supplementary Table S2.

The above key qCT variables at each visit and their changes between visits are presented in Table 3; Supplementary Table S3. Across all visits, Subjects 2 and 5 exhibited higher $fSAD\%_{Total}$ and $Emph\%_{Total}$ compared to the other subjects. Subjects 1, 3, and 4 showed moderate $fSAD\%_{Total}$, while Subjects 6 through 8 had low $fSAD\%_{Total}$. Within the subgroups (Halpin et al., 2022; Ferrera et al., 2021; Vogelmeier et al., 2020) and (Smith et al., 2018; Smith et al., 2020; Alford et al., 2010), $Emph\%_{Total}$ was mild for all subjects except Subject 3.

Association between SPECT and qCT variables

Association tests between SPECT and qCT variables were conducted using both cross-sectional and longitudinal data. The cross-sectional tests captured inter-subject variation, while the longitudinal tests tracked intra-subject progression. In the cross-sectional analysis, the SPECT variables CV_{Total} and TC_{Max} showed the strongest correlations with the qCT variables $fSAD\%_{Total}$ and $Emph\%_{Total}$. Specifically, CV_{Total} correlated 0.90 with $fSAD\%_{Total}$ and 0.71 with $Emph\%_{Total}$. Similarly, TC_{Max} correlated 0.86 with $fSAD\%_{Total}$ and 0.77 with $Emph\%_{Total}$. This association is visually illustrated in Figure 4, which compares the fSAD-pixel maps on CT coronal slices at V1 with TC distributions in the SPECT images. The relationship between qCT-based fSAD maps and SPECT-based ventilation patterns is particularly evident in the grouping of Subjects (Global Strategy for Prevention, 2023; Israel et al., 2019), (Halpin et al., 2022; Ferrera et al., 2021; Vogelmeier et al., 2020), and (Smith et al., 2018; Smith et al., 2020; Alford et al.,

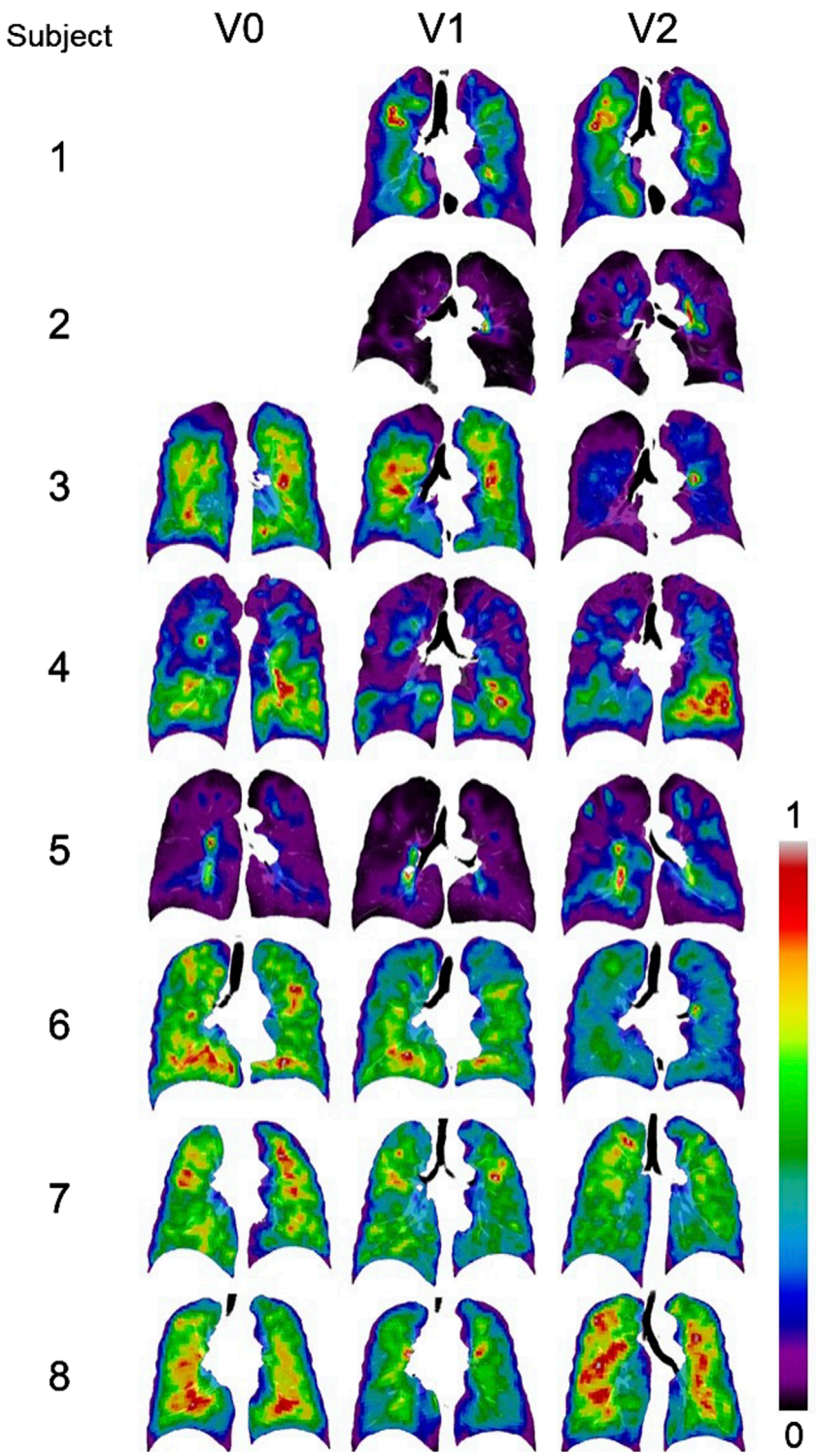

FIGURE 3
Normalized SPECT images transformed to the TLC domain at three visits. Subjects 1 and 2 did not have ventilation scans at V0. Intensities were normalized using the minimum and maximum values, resulting in contour values ranging from 0 to 1. The localized red spots in Subjects 2 and 5 indicate high-intensity hot spots where inhaled aerosols tend to deposit.

2010), which correspond to high, moderate, and low $fSAD\%_{Total}$, respectively. Importantly, participants who had more compromised lung function (specifically participants 2, 3, and 5) showed $\Delta V^{F}_{air,UML}$ values exceeding 1 throughout all visits, as indicated in Table 3.

In the longitudinal analysis, the correlations between the 1-year changes in SPECT variables and the corresponding changes in qCT variables were weak. However, over 2 years, TC_{Max} exhibited strong correlations with several qCT variables, including $fSAD\%_{Total}$

TABLE 2 CV_{Total} and TC_{Max} at each visit and their changes between visits.

Subject	V0	V1	V2	V1-V0	V2-V1	V2-V0
CV_{Total}						
1		0.73	0.75		0.02	
2		1.69	1.42		−0.27	
3	0.59	0.61	0.7	0.02	0.09	0.11
4	0.66	0.86	0.78	0.2	−0.08	0.13
5	0.94	1.18	0.93	0.24	−0.25	0
6	0.46	0.48	0.47	0.03	−0.02	0.01
7	0.55	0.58	0.48	0.04	−0.1	−0.07
8	0.53	0.57	0.54	0.03	−0.02	0.01
Mean ± SD	0.62 ± 0.15	0.84 ± 0.38	0.76 ± 0.29	0.09 ± 0.09	−0.08 ± 0.12	0.03 ± 0.07
TC_{Max}						
1		7.27	5.36		−1.91	
2		37.69	20.83		−16.86	
3	7.32	5.36	16.33	−1.97	10.97	9.01
4	5.03	14.22	7.82	9.19	−6.4	2.79
5	24.1	18.66	19.59	−5.44	0.93	−4.51
6	3.51	4.19	9.23	0.68	5.05	5.72
7	4.14	5	4.2	0.86	−0.81	0.06
8	3.82	4.21	3.55	0.39	−0.65	−0.26
Mean ± SD	7.99 ± 7.31	12.07 ± 10.88	10.87 ± 6.57	0.62 ± 4.41	−1.21 ± 7.62	2.14 ± 4.37

($r = -0.70$), $D^{*}_{h,sLUL}$ ($r = -0.74$), $Emph\%_{Total}$ ($r = -0.75$), and $\Delta V^{F}_{air,UML}$ ($r = 0.75$) (Figure 5). Additionally, the change (V2-V0) in $D^{*}_{h,sLUL}$ showed a moderate correlation with the change in $fSAD\%_{Total}$ ($r = 0.61$), while the change (V2-V0) in $\Delta V^{F}_{air,UML}$ was moderately correlated with the change in $Emph\%_{Total}$ ($r = -0.63$) (Supplementary Figure S2).

A *post hoc* study was conducted to establish the causal relationship between fSAD and heterogeneity of lung ventilation. Cross-lagged panel analysis, which is commonly used to infer the direction and strength of a relationship between two variables measured repeatedly at different time points, was employed (Kenny, 1975). The imaging variables of $fSAD\%_{Total}$ and CV_{Total} at V1 and V2 were selected for analysis since they were strongly correlated at all visits. The type one error rate (α) was set at 0.05. As demonstrated in Figure 6, two synchronous correlations ($r_{fSAD1,CV1}$ and $r_{fSAD2,CV2}$) and two stability correlations ($r_{CV1,CV2}$ and $r_{fSAD1,fSAD2}$) were significantly greater than zero, indicating that the assumptions of synchronicity and stationarity were not violated. For the cross-lagged correlations ($r_{fSAD1,CV2}$ and $r_{CV1,fSAD2}$), $r_{fSAD1,CV2}$ was significantly greater than zero while $r_{CV1,fSAD2}$ was not, suggesting that fSAD is the cause of heterogeneity of lung ventilation. Note that the cross-lagged correlations were partial correlations, with the contributions of the stability correlations partialled out. In COPD, the narrowing of small airways leads to higher airflow resistance and greater particle deposition in the lungs (Marsh et al., 2006; Kim and Kang, 1997; Zhang et al., 2022a). As a result, subjects with higher $fSAD\%_{Total}$ were observed to have localized areas of elevated TC activity.

Discussion

This longitudinal study successfully enrolled eight COPD subjects for three visits to examine cross-sectional and longitudinal relationships between qCT and SPECT biomarkers in COPD. Cross-sectional relationships reflect associations between variables at a single time point, whereas longitudinal relationships describe changes in these variables over time. Our analysis revealed strong positive cross-sectional correlations between SPECT-measured

10.3389/fphys.2025.1555230

TABLE 3 The selected qCT variables at each visit and their changes between visits.

Subject	V0	V1	V2	V1-V0	V2-V1	V2-V0
$fSAD\%_{Total}$						
1	12.49	14.3	12.52	1.81	−1.78	0.03
2	34.01	32.71	31.15	−1.3	−1.56	−2.86
3	13.55	13.13	12.26	−0.42	−0.87	−1.29
4	11.29	11.13	8.46	−0.16	−2.67	−2.84
5	22.83	21.3	24.86	−1.53	3.55	2.03
6	1.36	0.93	0.64	−0.43	−0.3	−0.73
7	0.65	0.8	0.35	0.16	−0.45	−0.3
8	0.53	0.96	1.37	0.43	0.41	0.84
Mean ± SD	12.09 ± 11.06	11.91 ± 10.56	11.45 ± 10.73	−0.18 ± 0.98	−0.46 ± 1.76	−0.64 ± 1.58
$D_{h,sLUL}{}^{*}$						
1	0.21	0.21	0.21	0	0	0
2	0.23	0.18	0.23	−0.05	0.05	0
3	0.23	0.14	0.22	−0.09	0.09	−0.01
4	0.21	0.2	0.21	−0.01	0.01	0
5	0.25	0.21	0.31	−0.03	0.1	0.06
6	0.28	0.27	0.25	−0.01	−0.01	−0.02
7	0.26	0.3	0.24	0.04	−0.06	−0.02
8	0.22	0.24	0.25	0.02	0.01	0.02
Mean ± SD	0.24 ± 0.02	0.22 ± 0.05	0.24 ± 0.03	−0.02 ± 0.04	0.02 ± 0.05	0 ± 0.03
$Emph\%_{Total}$						
1	3.15	7.57	8.47	4.42	0.9	5.32
2	27.12	29.64	29.37	2.52	−0.27	2.25
3	18.14	18.65	15.93	0.51	−2.72	−2.21
4	3.43	3.31	3.88	−0.12	0.58	0.46
5	39.36	40.42	41.1	1.06	0.68	1.74
6	3.39	4.25	4.32	0.86	0.06	0.92
7	0.9	0.65	0.75	−0.25	0.1	−0.15
8	4.97	6.51	7.07	1.53	0.56	2.1
Mean ± SD	12.56 ± 13.28	13.87 ± 13.46	13.86 ± 13.34	1.32 ± 1.44	−0.01 ± 1.09	1.3 ± 2.04
$\Delta V^{F}_{air,UML}$						
1	0.54	0.46	0.54	−0.08	0.08	0
2	1.43	1.68	1.91	0.25	0.24	0.48

(Continued on the following page)

10.3389/fphys.2025.1555230

TABLE 3 (*Continued*) The selected qCT variables at each visit and their changes between visits.

Subject	V0	V1	V2	V1-V0	V2-V1	V2-V0
3	1.44	1.59	2.61	0.14	1.02	1.17
4	0.61	0.62	0.7	0.02	0.08	0.1
5	1.22	1.3	1.2	0.07	−0.09	−0.02
6	0.92	0.85	1	−0.08	0.15	0.08
7	0.6	0.59	0.7	−0.01	0.11	0.1
8	0.55	0.54	0.56	−0.01	0.02	0.01
Mean ± SD	0.91 ± 0.37	0.95 ± 0.46	1.15 ± 0.69	0.04 ± 0.1	0.2 ± 0.32	0.24 ± 0.38

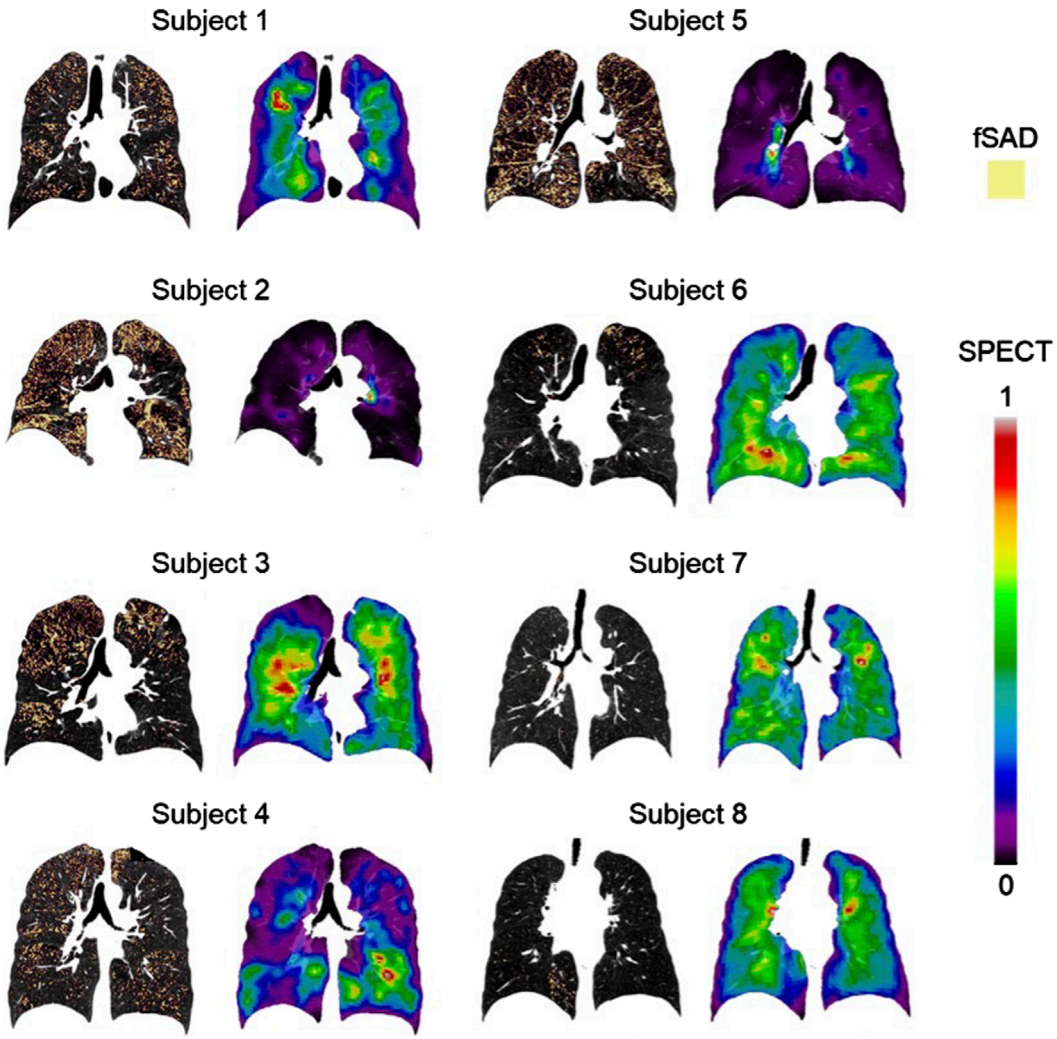

FIGURE 4
The fSAD-voxel maps (left column) and normalized TC SPECT images (right column) for each subject at V1, where fSAD stands for functional small airway disease and TC represents tracer concentration. These images were plotted in the coronal planes of the CT images. The relationship between qCT-based fSAD maps and SPECT-based ventilation patterns reveals distinct groupings among subjects: Subjects 2 and 5 exhibit high fSAD%$_{Total}$, Subjects 1, 3, and 4 display moderate fSAD%$_{Total}$, and Subjects 6, 7, and 8 demonstrate low fSAD%$_{Total}$. SPECT intensities were normalized using the minimum and maximum values, resulting in contour values ranging from 0 to 1.

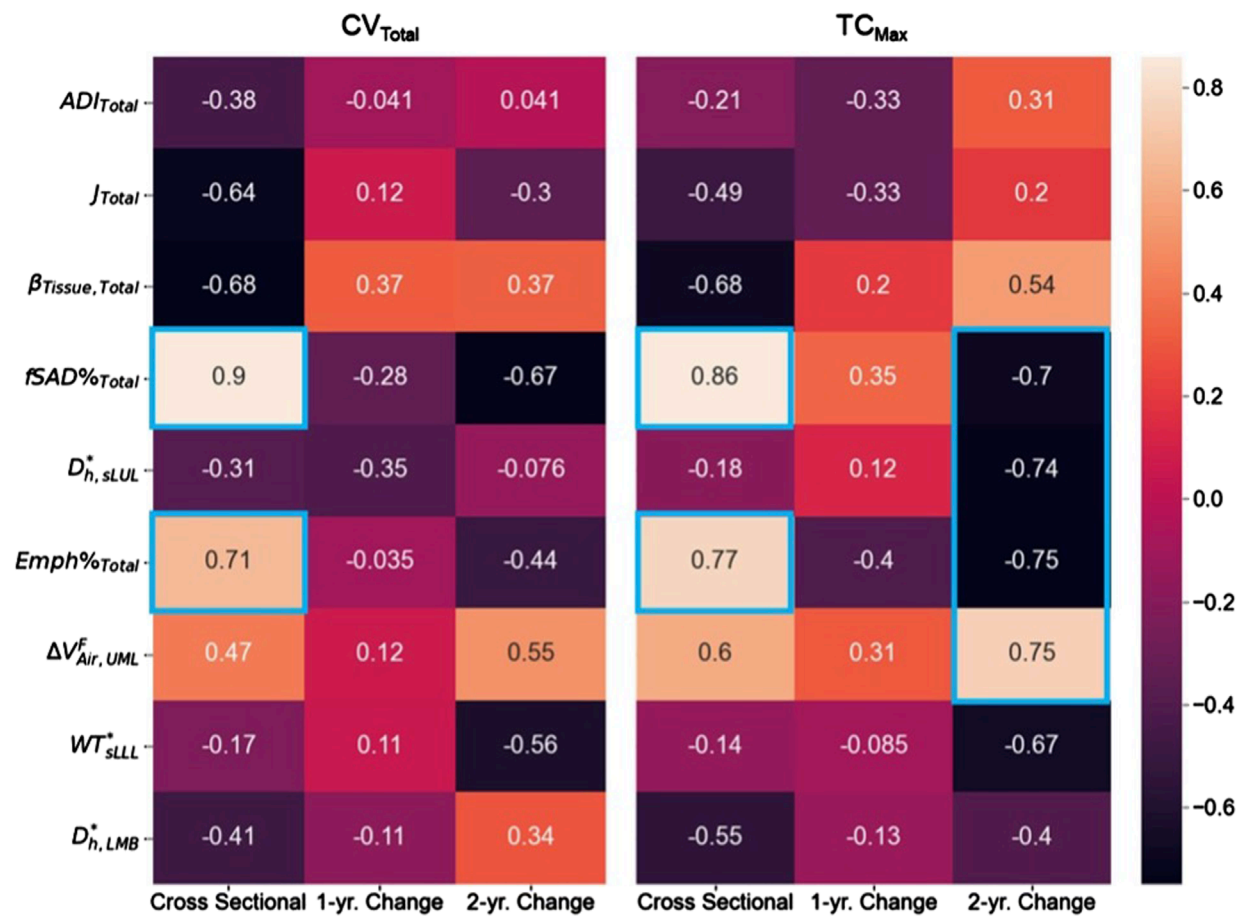

FIGURE 5
The correlation maps between the SPECT variables and the qCT variables for both cross-sectional and longitudinal data. Correlation magnitudes exceeding 0.7 were highlighted using blue boxes.

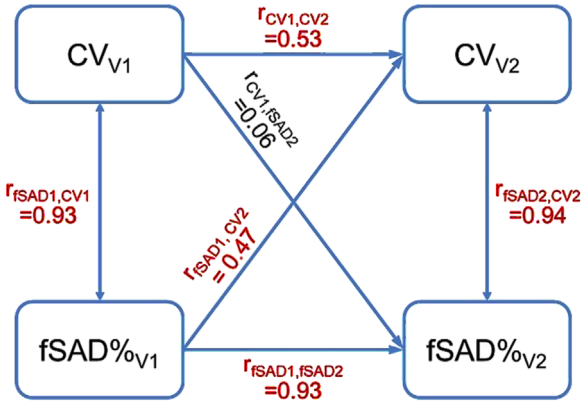

FIGURE 6
The cross-lagged panel analysis estimated a total of six correlations. The correlations colored in red were significantly greater than zero. The result that $r_{fSAD1,CV2}$ was greater than zero suggested that fSAD cause the heterogeneity of lung ventilation.

ventilation heterogeneity (CV_{Total}) and qCT-derived functional small airway disease ($fSAD\%_{Total}$) and emphysema ($Emph\%_{Total}$), suggesting that both small airway abnormalities and parenchymal destruction contribute to ventilation abnormalities in COPD, reflecting disease severity. Longitudinally, changes in TC_{Max} exhibited strong negative correlations with changes in $fSAD\%_{Total}$, $Emph\%_{Total}$, and average airway diameter, as well as a strong positive correlation with changes in lobar airflow distribution. These findings suggest that longitudinal changes in TC_{Max} may serve as a more sensitive biomarker for capturing the dynamic process of hot spot formation, independent of disease severity.

To our knowledge, this study is the first longitudinal CT/SPECT analysis to provide insights into COPD progression. The novelty of this study lies in its comprehensive qCT-based phenotyping at both local (segmental) and global (whole-lung) scales, the integration of dual imaging modalities, and its longitudinal design.

Association between imaging variables and PFTs

The strong correlation observed between TC% and ΔV^F_{air} of the lobes (Figure 2: r = 0.73) indicated that qCT-based ΔV^F_{air} can serve as a viable alternative for measuring lobar ventilation. This correlation also validates the effectiveness of the registration process utilized to align SPECT and CT images. Furthermore, significant negative

correlations were found between TC heterogeneity (CV_{Total}) and PFT results (Figure 2: r = −0.74 with FEV_1% predicted; r = −0.80 with FEV_1/FVC (%)), agreeing with previous studies (r = −0.84 to −0.89 with FEV_1% predicted) (Xu et al., 2001; Doganay et al., 2019).

Association between SPECT and qCT variables

The SPECT variables CV_{Total} and TC_{Max} showed strong correlations with the qCT variables $fSAD\%_{Total}$ (CV_{Total}: r = 0.90; TC_{Max}: r = 0.86) and $Emph\%_{Total}$ (CV_{Total}: r = 0.71; TC_{Max}: r = 0.77) in the cross-sectional data. This indicates that both small airway disease and emphysema are associated with lung ventilation heterogeneity, with small airway disease showing a stronger correlation.

Analysis of the longitudinal data collected over 2 years revealed strong correlations between TC_{Max} and $D_{h,sLUL}^{*}$ (r = −0.74) as well as $\Delta V_{air}{}^{F}{}_{UML}$ (r = 0.75) (Figure 5). These findings suggest that reduced diameters of segmental airways and imbalances in ventilation between the upper and lower lobes may contribute to the development of TC hot spots. In human anatomy, the lower lobes of the lungs are generally larger than the upper lobes in terms of volume (Yamada et al., 2020). Notably, subjects with more impaired lung function (subjects 2, 3, and 5) consistently demonstrated $\Delta V^{F}_{air,UML}$ values greater than 1 across all visits (Table 3), suggesting compensatory mechanisms where ventilation shifts preferentially to the upper lobes rather than the lower lobes. Visual inspection of the segmental airways in the LUL of Subjects 3 and 5 showed constricted branches at V2 and V0, respectively (Figure 7). This observation highlights the negative correlations between changes in $D_{h,sLUL}^{*}$ and changes in SPECT ventilation images, supporting a previous study identifying $D_{h,sLUL}^{*}$ as a significant qCT variable in characterizing COPD subjects (Haghighi et al., 2019a).

Furthermore, changes in TC_{Max} over 2 years were negatively correlated with changes in fSAD% (r = −0.70) and Emph% (r = −0.75) (Figure 5). This suggests that variations in $D_{h,sLUL}^{*}$ and $\Delta V^{F}_{air,UML}$ may moderate the relationship between changes in TC_{Max} and changes in $fSAD\%_{Total}$ and $Emph\%_{Total}$, particularly when disease progression, in terms of COPD stages, remains relatively stable. Namely, $Emph\%_{Total}$ and $fSAD\%_{Total}$ progression may experience airway collapse/alveolar destruction, which contribute less to overall ventilation and redistribute airflow to less affected areas. These findings indicate that the formation of hot spots in COPD patients could be influenced by alterations in segmental airways in the left upper lobe (Figure 7), as well as changes in airflow distribution between the upper and lower lobes, in addition to factors such as fSAD and emphysema.

Interestingly, the correlations between TC_{Max} and both fSAD% and Emph% in the longitudinal data differed from those in the cross-sectional data. Cross-sectional correlations reflect static disease phenotypes and severity at a single time point, whereas longitudinal correlations capture changes in variables over 2 years, independent of severity. These findings align with Zou et al. (2021a)'s distinction between cross-sectional and longitudinal analyses, where "cross-sectional clustering was based on static disease stage (severity)" while "longitudinal clustering aims to identify COPD progression clusters, which are more dependent upon disease progression than severity." In our data, cross-sectional correlations capture disease severity, with increased small airway disease and emphysema leading to greater ventilation heterogeneity. However, longitudinally, areas with high TC_{Max} may experience reduced progression of fSAD and emphysema, possibly due to compensatory mechanisms or a plateau in disease progression. These findings suggest that studies investigating COPD progression should consider not only severity markers but also progression patterns identified through longitudinal imaging.

The U.S. National Institutes of Health (NIH) has sponsored multi-center trials, such as the Genetic Epidemiology of COPD study (COPDGene) (Regan et al., 2010; Regan et al., 2019) and the SubPopulations and InteRmediate Outcome Measures in COPD Study (SPIROMICS) (Couper et al., 2014; Woodruff et al., 2015), to collect comprehensive clinical, biologic, genetic, and CT data across large populations. These efforts aim to uncover novel disease pathways, identify surrogate markers of severity, define endotypes, predict health trajectories, and inform clinical trial and treatment strategies. Additionally, these large datasets present both opportunities and challenges for advancing analytical, computational, and machine learning methods in complex biological systems (Peng et al., 2021; Alber et al., 2019; Lin et al., 2021). For example, based on COPDGene data, several novel COPD subgroups and pathways have been identified (Young et al., 2019a; Young et al., 2019b), including an airway-predominant disease subgroup progressing from GOLD 0 to preserved ratio-impaired spirometry (PRISm) status, and an emphysema-predominant disease subgroup progressing from GOLD 0 to GOLD 1 status.

Furthermore, based on SPIROMICS data, qCT-based clusters have been identified in both current and former smokers (Haghighi et al., 2018c; Haghighi et al., 2019b), with additional longitudinal qCT-based clusters identified in former smokers (Zou et al., 2021b). Deep learning approaches have also been developed to identify lung tissue pattern clusters, their latent traits, and associations with drug use in COPD patients (Li et al., 2021). In addition, a CT-based, subject-specific computational fluid and particle dynamics (CFPD) model for the whole lung has also been developed and applied to post-COVID-19 subjects to explore airway resistance and particle deposition across different subgroups (Zhang et al., 2022b; Zhang et al., 2024).

The ultimate goal of this study is to bridge the gaps between big data (including clinical and imaging data), artificial intelligence (machine learning and deep learning), and advanced computational models. The specific objective was to explore the connections between qCT-based variables and SPECT-measured ventilation features, both cross-sectionally and longitudinally. In future studies, the findings summarized below can be used to assess the sensitivity of the CFPD model in predicting SPECT-measured ventilation biomarkers across various COPD severities in both former and current smokers, aiding model validation and data interpretation. The validated CFPD model can then be applied to predict the deposition of inhaled particles of various sizes in conducting and respiratory airways with different breathing patterns, thereby improving tailored inhalational therapies. For example, subgroup-specific inhalers or inhalational waveforms could be developed to target different regions of the lung for optimal deposition efficiency and improved clinical outcomes.

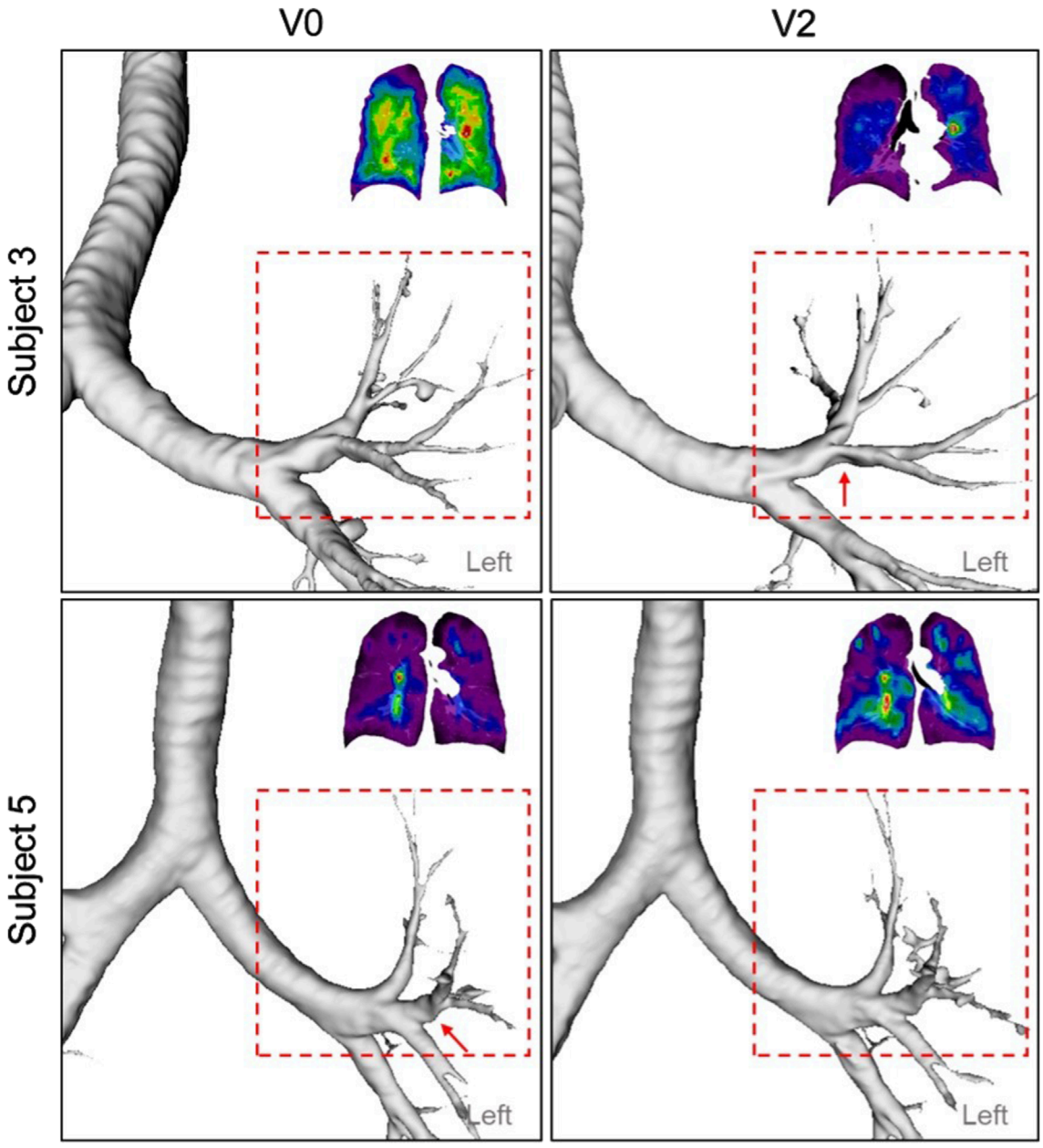

FIGURE 7
A constricted segmental airway in the LUL (red arrow) of Subject 3 at V2, which may contribute to the TC hot spot observed in the same region. In addition, a constricted segmental airway in the LUL (red arrow) of Subject 5, present at V0, had resolved by V2, potentially increasing ventilation homogeneity.

This study had several limitations. Firstly, the spatial resolution of SPECT images (3.985 mm) is lower than that of CT scans (0.5–0.7 mm), which may lead to inaccuracies in quantifying certain regions on SPECT images. Additionally, subjects were exposed to radiation during SPECT imaging, although the dose was within safety limits. Recently approved by the FDA, hyperpolarized xenon-129 magnetic resonance imaging (XeMRI) offers an alternative method for assessing lung ventilation distribution without exposing patients to ionizing radiation (Doganay et al., 2019; Peiffer et al., 2023; Kim et al., 2019; Bayat et al., 2023). Secondly, the strong correlations observed ($|r| > 0.70$) suggest large effect sizes, indicating potentially meaningful relationships between qCT and SPECT variables, despite the small sample size. Nonetheless, increasing the sample size and distinguishing current smokers from non-smokers is essential for achieving more robust and reliable results. Lastly, the subjects in this study effectively managed their disease over the 2-year period, with no significant changes in lung function. To gain a clearer understanding of COPD progression, it may be necessary to extend the interval between visits beyond the 2-year period.

Although this study was limited by a small sample size, our analysis suggests that SPECT ventilation imaging can effectively capture ventilation heterogeneity in COPD patients and provide complementary insights when paired with CT-based biomarkers. Specifically, SPECT images identified three distinct categories of subjects: severe COPD (Subjects 2 and 5), moderate COPD (Subjects 1, 3, and 4), and those with mild symptoms or at risk of developing COPD (Subjects 6, 7, and 8). Our findings indicate that small airway disease plays a crucial role in the heterogeneous ventilation observed in COPD patients. Additionally, the formation of hot spots in COPD could be influenced by changes in the segmental airways of the left upper lobe, alternations in airflow distribution between the upper and lower lobes, and the extent of small airway disease and emphysema. Further research into small airway disease could enhance our understanding of COPD's diverse characteristics, aid in the identification of novel phenotypes across various imaging modalities and offer deeper insights into the disease's progression.

Data availability statement

The original contributions presented in the study are included in the article/Supplementary Material, further inquiries can be directed to the corresponding author.

Ethics statement

The studies involving humans were approved by the institutional review board of the University of Iowa. The studies were conducted in accordance with the local legislation and institutional requirements. The participants provided their written informed consent to participate in this study.

Author contributions

FL: Conceptualization, Data curation, Formal Analysis, Investigation, Methodology, Project administration, Resources, Software, Validation, Visualization, Writing – original draft, Writing – review and editing. XZ: Conceptualization, Formal Analysis, Investigation, Software, Writing – original draft, Writing – review and editing. AC: Conceptualization, Funding acquisition, Resources, Supervision, Writing – original draft, Writing – review and editing. EH: Conceptualization, Funding acquisition, Resources, Supervision, Writing – original draft, Writing – review and editing. MG: Conceptualization, Funding acquisition, Methodology, Resources, Writing – original draft, Writing – review and editing. C-LL: Conceptualization, Formal Analysis, Funding acquisition, Investigation, Methodology, Project administration, Resources, Supervision, Validation, Writing – original draft, Writing – review and editing.

Funding

The author(s) declare that financial support was received for the research and/or publication of this article. Supports for this study were provided, in part, by NIH grants R01-HL168116, U01-HL114494, R01-HL112986, S10-RR022421, T32-HL144461, and ED grant P116S210005.

Acknowledgments

The authors extend their sincere gratitude to Dr. Prathish K. Rajaraman for his invaluable expertise and insightful contributions, which significantly enhanced the quality and depth of this manuscript during the revision process.

Conflict of interest

The authors declare that the research was conducted in the absence of any commercial or financial relationships that could be construed as a potential conflict of interest.

The author(s) declared that they were an editorial board member of Frontiers, at the time of submission. This had no impact on the peer review process and the final decision.

Generative AI statement

The author(s) declare that Generative AI was used in the creation of this manuscript. Generative AI was used to fix the grammar and improve the language.

Publisher's note

Supplementary material

The Supplementary Material for this article can be found online at: https://www.frontiersin.org/articles/10.3389/fphys.2025.1555230/full#supplementary-material

References

Akoglu, H. (2018). User's guide to correlation coefficients. *Turk J. Emerg. Med.* 18 (3), 91–93. doi:10.1016/j.tjem.2018.08.001

Alber, M., Buganza Tepole, A., Cannon, W. R., De, S., Dura-Bernal, S., Garikipati, K., et al. (2019). "Integrating machine learning and multiscale modeling—perspectives,

challenges, and opportunities in the biological, biomedical, and behavioral sciences," 2. United Kingdom: Nature Research. npj Digital Medicine. doi:10.1038/s41746-019-0193-y

Alford, S. K., Van Beek, E. J. R., McLennan, G., and Hoffman, E. A. (2010). Heterogeneity of pulmonary perfusion as a mechanistic image-based phenotype in emphysema susceptible smokers. *Proc. Natl. Acad. Sci. U. S. A.* 107 (16), 7485–7490. doi:10.1073/pnas.0913880107

Bayat, S., Wild, J., and Winkler, T. (2023). Lung functional imaging. *Breathe* 19 (3), 220272. doi:10.1183/20734735.0272-2022

Choi, S., Hoffman, E. A., Wenzel, S. E., Castro, M., Fain, S. B., Jarjour, N. N., et al. (2015). Quantitative assessment of multiscale structural and functional alterations in asthmatic populations. *J. Appl. Physiol.* 118 (10), 1286–1298. doi:10.1152/japplphysiol.01094.2014

Cohen, J. (1992). A power primer. *Psychol. Bull.* 112 (1), 155–159. doi:10.1037//0033-2909.112.1.155

Couper, D., LaVange, L. M., Han, M. L., Barr, R. G., Bleecker, E., Hoffman, E. A., et al. (2014). Design of the subpopulations and intermediate outcomes in copd study (SPIROMICS). *Thorax* 69 (5), 491–494. doi:10.1136/thoraxjnl-2013-203897

De Backer, J. W., Vos, W. G., Vinchurkar, S. C., Claes, R., Drollmann, A., Wulfrank, D., et al. (2010). Validation of computational fluid dynamics in CT-based airway models with SPECT/CT. *Radiology* 257 (3), 854–862. doi:10.1148/radiol.10100322

Doganay, O., Matin, T., Chen, M., Kim, M., McIntyre, A., McGowan, D. R., et al. (2019). Time-series hyperpolarized xenon-129 MRI of lobar lung ventilation of COPD in comparison to V/Q-SPECT/CT and CT. *Eur. Radiol.* 29 (8), 4058–4067. doi:10.1007/s00330-018-5888-y

Ferrera, M. C., Labaki, W. W., and Han, M. K. (2021). Advances in chronic obstructive pulmonary disease. *Annu. Rev. Med.* 72, 119–134. doi:10.1146/annurev-med-080919-112707

Fuld, M. K., Grout, R. W., Guo, J., Morgan, J. H., and Hoffman, E. A. (2012). Systems for lung volume standardization during static and dynamic MDCT-based quantitative assessment of pulmonary structure and function. *Acad. Radiol.* 19 (8), 930–940. doi:10.1016/j.acra.2012.03.017

Galbán, C. J., Han, M. K., Boes, J. L., Chughtai, K. A., Meyer, C. R., Johnson, T. D., et al. (2012). Computed tomography-based biomarker provides unique signature for diagnosis of COPD phenotypes and disease progression. *Nat. Med.* 18 (11), 1711–1715. doi:10.1038/nm.2971

GLOBAL STRATEGY FOR PREVENTION (2023). DIAGNOSIS and management of COPD: 2023 report.

Haghighi, B., Choi, S., Choi, J., Hoffman, E. A., Comellas, A. P., Newell, J. D., et al. (2018a). Imaging-based clusters in current smokers of the COPD cohort associate with clinical characteristics: the SubPopulations and Intermediate Outcome Measures in COPD Study (SPIROMICS). *Respir. Res.* 19 (1), 178. doi:10.1186/s12931-018-0888-7

Haghighi, B., Choi, S., Choi, J., Hoffman, E. A., Comellas, A. P., Newell, J. D., et al. (2018c). Imaging-based clusters in current smokers of the COPD cohort associate with clinical characteristics: the SubPopulations and Intermediate Outcome Measures in COPD Study (SPIROMICS). *Respir. Res.* 19 (1), 178. doi:10.1186/s12931-018-0888-7

Haghighi, B., Choi, S., Choi, J., Hoffman, E. A., Comellas, A. P., Newell, J. D., et al. (2019a). Imaging-based clusters in former smokers of the COPD cohort associate with clinical characteristics: the SubPopulations and intermediate outcome measures in COPD study (SPIROMICS). *Respir. Res.* 20 (1), 153. doi:10.1186/s12931-019-1121-z

Haghighi, B., Choi, S., Choi, J., Hoffman, E. A., Comellas, A. P., Newell, J. D., et al. (2019b). Imaging-based clusters in former smokers of the COPD cohort associate with clinical characteristics: the SubPopulations and intermediate outcome measures in COPD study (SPIROMICS). *Respir. Res.* 20 (1), 153. doi:10.1186/s12931-019-1121-z

Haghighi, B., Ellingwood N, D., Yin, Y., Hoffman, E. A., and Lin, C. L. (2018b). A GPU-based symmetric non-rigid image registration method in human lung. *Med. Biol. Eng. Comput.* 56 (3), 355–371. doi:10.1007/s11517-017-1690-2

Halpin, D. M. G., Vogelmeier, C. F., and Agusti, A. (2022). Lung health for all: chronic obstructive lung disease and world lung day 2022. *Am. J. Respir. Crit. Care Med.* 206 (6), 669–671. doi:10.1164/rccm.202207-1407ED

Horn, J. (1965). Factors in factor analysis. *Psychometrika* 30 (2), 179–185. doi:10.1007/BF02289447

Israel, O., Pellet, O., Biassoni, L., De Palma, D., Estrada-Lobato, E., Gnanasegaran, G., et al. (2019). Two decades of SPECT/CT – the coming of age of a technology: an updated review of literature evidence. *Eur. J. Nucl. Med. Mol. Imaging* 46 (10), 1990–2012. doi:10.1007/s00259-019-04404-6

Iyer, K. S., Newell, J. D., Jin, D., Fuld, M. K., Saha, P. K., Hansdottir, S., et al. (2016). Quantitative dual-energy computed tomography supports a vascular etiology of smoking-induced inflammatory lung disease. *Am. J. Respir. Crit. Care Med.* 193 (6), 652–661. doi:10.1164/rccm.201506-1196OC

Kaiser, H. F. (1958). The varimax criterion for analytic rotation in factor analysis. *Psychometrika* 23 (3), 187–200. doi:10.1007/bf02289233

Kenny, D. A. (1975). Cross-lagged panel correlation: a test for spuriousness. *Psychol. Bull.* 82 (6), 887–903. doi:10.1037//0033-2909.82.6.887

Kim, C. S., and Kang, T. C. (1997). Comparative measurement of lung deposition of inhaled fine particles in normal subjects and patients with obstructive airway disease. *Am. J. Respir. Crit. Care Med.* 155 (3), 899–905. doi:10.1164/ajrccm.155.3.9117024

Kim, M., Doganay, O., Matin, T. N., Povey, T., and Gleeson, F. V. (2019). CT-based airway flow model to assess ventilation in chronic obstructive pulmonary disease: a pilot study. *Radiology* 293 (3), 666–673. doi:10.1148/radiol.2019190395

Krogsgaard, O. W. (1976). Technetium-99m-Sulfur colloid 5.

Li, F., Choi, J., Zou, C., Newell, Jr J. D., Comellas, A. P., Lee, C. H., et al. (2021). Latent traits of lung tissue patterns in former smokers derived by dual channel deep learning in computed tomography images. *Sci. Rep.* 11 (1), 4916. doi:10.1038/s41598-021-84547-5

Lin, C. L., Hoffman, E. A., and Kassinos, S. (2021). "Machine learning and *in silico* methods," in *Inhaled medicines* (Elsevier), 375–390.

Marsh, S., Aldington, S., Williams, M. V., Nowitz, M., Kingzett-Taylor, A., Weatherall, M., et al. (2006). Physiological associations of computerized tomography lung density: a factor analysis. *Int. J. Chron. Obstruct Pulmon Dis.* 1 (2), 181–187. doi:10.2147/copd.2006.1.2.181

Motahari, A., Barr, R. G., Han, M. L. K., Anderson, W. H., Barjaktarevic, I., Bleecker, E. R., et al. (2023). Repeatability of pulmonary quantitative computed tomography measurements in chronic obstructive pulmonary disease. *Am. J. Respir. Crit. Care Med.* 208 (6), 657–665. doi:10.1164/rccm.202209-1698PP

Nagao, M., and Murase, K. (2002). Measurement of heterogeneous distribution on Technegas SPECT images by three-dimensional fractal analysis. *Ann. Nucl. Med.* 16 (6), 369–376. doi:10.1007/BF02990073

Ostridge, K., Williams, N., Kim, V., Bennett, M., Harden, S., Welch, L., et al. (2016). Relationship between pulmonary matrix metalloproteinases and quantitative CT markers of small airways disease and emphysema in COPD. *Thorax* 71 (2), 126–132. doi:10.1136/thoraxjnl-2015-207428

Peiffer, J. D., Altes, T., Ruset, I. C., Hersman, F. W., Mugler, J. P., Meyer, C. H., et al. (2023). Hyperpolarized 129Xe MRI, 99mTc scintigraphy, and SPECT in lung ventilation imaging: a quantitative comparison. *Acad. Radiol.*, 1–10. doi:10.1016/j.acra.2023.10.038

Pellegrino, R., Viegi, G., Brusasco, V., Crapo, R. O., Burgos, F., Casaburi, R., et al. (2005). Interpretative strategies for lung function tests. *Eur. Respir. J.* 26 (5), 948–968. doi:10.1183/09031936.05.00035205

Peng, G. C. Y., Alber, M., Buganza Tepole, A., Cannon, W. R., De, S., Dura-Bernal, S., et al. (2021). Multiscale modeling meets machine learning: what can we learn? *Archives Comput. Methods Eng.* 28 (3), 1017–1037. doi:10.1007/s11831-020-09405-5

Regan, E. A., Hersh, C. P., Castaldi, P. J., DeMeo, D. L., Silverman, E. K., Crapo, J. D., et al. (2019). Omics and the search for blood biomarkers in chronic obstructive pulmonary disease. Insights from COPDGene. *Am. J. Respir. Cell Mol. Biol.* 61, 143–149. doi:10.1165/rcmb.2018-0245PS

Regan, E. A., Hokanson, J. E., Murphy, J. R., Make, B., Lynch, D. A., Beaty, T. H., et al. (2010). Genetic epidemiology of COPD (COPDGene) study design. *COPD J. Chronic Obstr. Pulm. Dis.* 7 (1), 32–43. doi:10.3109/15412550903499522

Shreffler, J., and Huecker, M. R. (2023). "Type I and type II errors and statistical power," in *StatPearls* (Treasure island, FL: StatPearls Publishing). Available online at: https://www.ncbi.nlm.nih.gov/books/NBK557530/.

Singh, D. (2017). Small airway disease in patients with chronic obstructive pulmonary disease. *Tuberc. Respir. Dis. Seoul.* 80 (4), 317–324. doi:10.4046/trd.2017.0080

Sirr, S. A., Juenemann, P. J., Tom, H., Boudreau, R. J., Chandler, R. P., and Loken, M. K. (1985). Effect of ethanol on droplet size, efficiency of delivery, and clearance characteristics of technetium-99m DTPA aerosol. *J. Nucl. Med.* 26 (6), 643–646.

Smith, B. M., Kirby, M., Hoffman, E. A., Kronmal, R. A., Aaron, S. D., Allen, N. B., et al. (2020). Association of dysanapsis with chronic obstructive pulmonary disease among older adults. *JAMA - J. Am. Med. Assoc.* 323 (22), 2268–2280. doi:10.1001/jama.2020.6918

Smith, B. M., Traboulsi, H., Austin, J. H. M., Manichaikul, A., Hoffman, E. A., Bleecker, E. R., et al. (2018). Human airway branch variation and chronic obstructive pulmonary disease. *Proc. Natl. Acad. Sci. U. S. A.* 115 (5), E974–E981. doi:10.1073/pnas.1715564115

Vogelmeier, C. F., Román-Rodríguez, M., Singh, D., Han, M. L. K., Rodríguez-Roisin, R., and Ferguson, G. T. (2020). Goals of COPD treatment: focus on symptoms and exacerbations. *Respir. Med.* 166 (March), 105938. doi:10.1016/j.rmed.2020.105938

Woodruff, P. G., Agusti, A., Roche, N., Singh, D., and Martinez, F. J. (2015). Current concepts in targeting chronic obstructive pulmonary disease pharmacotherapy: making progress towards personalised management. *Lancet* 385 (9979), 1789–1798. doi:10.1016/S0140-6736(15)60693-6

Xu, J., Moonen, M., Johansson, Å., Gustafsson, A., and Bake, B. (2001). Quantitative analysis of inhomogeneity in ventilation SPET. *Eur. J. Nucl. Med.* 28 (12), 1795–1800. doi:10.1007/s002590100649

Yamada, Y., Yamada, M., Yokoyama, Y., Tanabe, A., Matsuoka, S., Niijima, Y., et al. (2020). Differences in lung and lobe volumes between supine and standing positions scanned with conventional and newly developed 320-detector-row upright CT: intra-individual comparison. *Respiration* 99 (7), 598–605. doi:10.1159/000507265

Young, K. A., Regan, E. A., Han, M. L. K., Lutz, S. M., Ragland, M., Castaldi, P. J., et al. (2019a). Subtypes of COPD have unique distributions and differential risk of mortality. *Chronic Obstr. Pulm. Dis.* 6 (5), 400–413. doi:10.15326/jcopdf.6.5.2019.0150

Young, K. A., Strand, M. J., Ragland, M. F., Kinney, G. L., Austin, E. E., Regan, E. A., et al. (2019b). Pulmonary subtypes exhibit differential global initiative for chronic obstructive lung disease spirometry stage progression: the COPDGene® study. *Chronic Obstr. Pulm. Dis.* 6 (5), 414–429. doi:10.15326/jcopdf.6.5.2019.0155

Zhang, X., Li, F., Rajaraman, P. K., Choi, J., Comellas, A. P., Hoffman, E. A., et al. (2022a). A computed tomography imaging-based subject-specific whole-lung deposition model. *Eur. J. Pharm. Sci.* 177 (July), 106272. doi:10.1016/j.ejps.2022.106272

Zhang, X., Li, F., Rajaraman, P. K., Choi, J., Comellas, A. P., Hoffman, E. A., et al. (2022b). A computed tomography imaging-based subject-specific whole-lung deposition model. *Eur. J. Pharm. Sci.* 177 (July), 106272. doi:10.1016/j.ejps.2022.106272

Zhang, X., Li, F., Rajaraman, P. K., Comellas, A. P., Hoffman, E. A., and Lin, C. L. (2024). Investigating distributions of inhaled aerosols in the lungs of post-COVID-19 clusters through a unified imaging and modeling approach. *Eur. J. Pharm. Sci.* 195, 106724. doi:10.1016/j.ejps.2024.106724

Zou, C., Li, F., Choi, J., Haghighi, B., Choi, S., Rajaraman, P. K., et al. (2021a). Longitudinal imaging-based clusters in former smokers of the copd cohort associate with clinical characteristics: the subpopulations and intermediate outcome measures in copd study (spiromics). *Int. J. COPD* 16 (April), 1477–1496. doi:10.2147/COPD.S301466

Zou, C., Li, F., Choi, J., Haghighi, B., Choi, S., Rajaraman, P. K., et al. (2021b). Longitudinal imaging-based clusters in former smokers of the copd cohort associate with clinical characteristics: the subpopulations and intermediate outcome measures in copd study (spiromics). *Int. J. Chron. Obstruct Pulmon Dis.* 16, 1477–1496. doi:10.2147/COPD.S301466